A Report

entitled

ANALYTICAL STUDY OF TWIN-JET SHIELDING
ANNUAL PROGRESS REPORT

NASA Grant No. NAG 1-11

Submitted by the

TEXAS A & M RESEARCH FOUNDATION

to

National Aeronautics and Space Administration
Langely Research Center

Prepared by

Dr. Carl H. Gerhold

of the

Department of Mechanical Engineering
Texas A & M University
College Station, Texas 77843

December 31, 1980

TABLE OF CONTENTS

Analytical Study of Twin-Jet Shielding

I SUMMARY

This report summarizes the development of the analytical model of twin-jet shielding. The model consists of a point noise source impinging on a cylinder of heated flow in which the temperature and flow velocity are uniform across the cross-section.

In the formulation of the model, the wave equations are written for the regions outside the flow and within the flow cylinder. The solutions to the wave equations are matched at the jet boundary under the conditions of continuity of pressure and continuity of the vortex sheet. The solution reduces to an indefinite integral involving Bessel functions. The integral is solved approximately using a saddle point method.

The resulting model is analysed in order to identify the mechanisms of transmission and diffraction which control shielding in the shadow of the shielding jet. The impact that variations in jet operating parameters has on shielding is investigated. It is found that in the zone of the shadow region in which transmission dominates, shielding is relatively insensitive to variations of such parameters as Mach Number and spacing ratio. Comparison of the three-dimensional model to a previously obtained two-dimensional model shows good agreement.

In the zone in which diffraction dominates, shielding is more sensitive to variations in Mach Number, jet temperature and spacing ratio.

The model is found to compare to experimental shielding results. The major discrepancy between the model and experiment is felt to arise from the difference between the single point noise source of the model and the distributed source of the jet. Refinement of this noise source to a more realistic representation of the real jet is one of the goals of the continued effort in this project.

I INTRODUCTION

One of the drawbacks of the growing dependence on air travel is the increased impact of aircraft noise. Assessment and reduction of this impact requires identification of aircraft generated noise levels. To this end, the Noise Technology Branch of NASA/Aircraft Noise Reduction Division is developing and refining an aircraft noise prediction computer program. Noise estimation includes consideration not only of noise sources on the aircraft, but also of the propagation path between source and receiver. One of the numerous factors affecting the noise transmission path is shielding of one jet by another. The shielding jet, because of the high temperature and flow speed with respect to the immediate surroundings, acts as a partial barrier between the source and the receiver. The resultant noise reduction not only affects the overall aircraft noise level, but also indicates the possibility of jet engine installation as a means of aircraft noise control.

It is the purpose of this project to develop an analytical method to estimate the shielding of one jet by an adjacent jet in a twin jet configuration.

The problem of reflection and transmission of sound by a moving medium has been addressed assuming a plane wave incident on a plane interface (1,2,3,4). Ray tracing techniques have been applied to two-dimensional jets (5) and cold jets (6).

In this study, the three-dimensional case is considered. The model developed consists of the sound field emmited from a stationary, discrete frequency point source, which impinges on a cylinder of locally parallel flow. The temperature and velocity profiles are uniform in the jet at any location down stream of the nozzle. While this model is idealized, it is felt to incorporate the basic elements essential for a realistic representation; not only of the source, but also of the shielding jet.

The wave equations are written for the acoustic velocity potential in the region outside the jet and in the region within the jet. The equations incorporate the convective effect due to local mean flow. The velocity potentials in the two regions are matched at the flow boundary by the conditions of pressure continuity and continuity of the vortex sheet.

The solution for the acoustic pressure in the far field, which is derived from the velocity potential, is normalized by the incident acoustic pressure. This incident sound pressure is the sound pressure at the same location in the far field in the absence of the jet. This normalized sound pressure is related to the directivity.

The model is used to evaluate the effect on the far field noise radiation due to variations of such operating parameters as shielding jet flow speed and temperature, and the spacing between the source and the shielding jet.

III MODEL DEVELOPMENT

1. Formulation of the Model

The derivation of the model was shown in the first progress report (7). A summary of that derivation is shown below.

The mechanisms by which shielding occurs are reflection and refraction of sound at the boundary between the jet and the surrounding air and by diffraction around the jet.

The noise source is modelled by a stationary, discrete frequency point source located at (r_o, θ_o, o). The shielding jet is a cylinder of radius a, and is infinite in extent along the z-axis. The temperature and flow velocity are uniform across the cylinder cross-section. The model is illustrated in Figure 1. The expression for acoustic velocity potential is written for two regions; region I is outside the jet, region II is within the jet.

In region 1 (outside the flow-incident upon the shielding jet)

$$\nabla^2\phi - \frac{1}{c_o^2}\phi_{tt} = Q_o e^{-i\omega t}\,\delta(r-r_o)\,\delta(\theta-\theta_o)\,\delta(z) \qquad 1a)$$

In region I (outside the flow-reflected from the shielding Jet)

$$\nabla^2\phi - \frac{1}{c_o^2}\phi_{tt} = o \qquad 1b)$$

In region II (inside the flow)

$$\nabla^2\phi - M^2\phi_{zz} - \frac{2M}{c_1}\phi_{zt} - \frac{1}{c_1^2}\phi_{tt} = o \qquad 2)$$

Where:

$(r_o, \theta_o, o,)$ - location of point source

(r, θ, z) - location of the receiver

ω - source frequency

Q_o - source strength

c - sound speed

M - mach number - (jet flow speed/c_1)

$$\nabla^2\phi = \phi_{rr} + \frac{1}{r}\phi_r + \frac{1}{r^2}\phi_{\theta\theta} + \phi_{zz}$$

Note: The subscript o refers to conditions outside the flow (ambient), and 1 refers to conditions within the heated jet.

The boundary conditions at the interface between the ambient air and the jet are:

1) Pressure continuity

$$(p)_o = (p)_1 \quad \text{at } r = a$$

or-

$$-\rho_o(\phi_t)_o = -\rho_1(\phi_t + V\phi_z)_1 \quad \text{at } r = a \qquad 3)$$

2) Continuity of the vortex sheet (1,2). This condition states that the displacement of the medium is continuous and symmetrical at the boundary; r = a. Denoting this displacement by $\eta = (z,t)$, then:

$$\left.\frac{D\eta}{Dt}\right|_o = \left.\frac{D\eta}{Dt}\right|_1 \quad \text{at } r = a$$

or-

$$(\eta_t)_o = (\eta_t + V\eta_z)_1, \quad \text{at } r = a \qquad 4)$$

Time is eliminated from equations 1 and 2 by assuming:

$$\phi(r, \theta, z, t) = \psi(r, \theta, z)e^{-i\omega t}$$

The problem is reduced to a two-dimensional formulation by the Fourier transform:

$$\tilde{\psi} = \frac{1}{2\pi}\int_{-\infty}^{+\infty} \psi e^{-ik_z z}\, dz$$

with corresponding inverse:

$$\psi = \int_{-\infty}^{+\infty} \tilde{\psi} e^{ik_z z} dk_z$$

Solution of the transformed equations, inclusion of the boundary conditions and inverse transformations yields the equation for the acoustic velocity potential in the far field (r>>a):

$$\phi = \frac{-iQ_o e^{-i\omega t}}{8\pi} \sum_{m=o}^{\infty} \epsilon_m \cos m(\theta-\theta_o) \int_{-\infty}^{+\infty} H_m(K_o r)\, F_m(K_o,K_1) e^{ik_z(z)} dk_z \qquad 5)$$

where:

$$F_m(K_o,K_1) = J_m(K_o r) - \frac{H_m(K_o r_o)[J_m(K_1 a)J_m'(K_o a) - TJ_m(K_o a)J_m'(K_1 a)]}{TH_m(K_o a)J_m'(K_1 a) - J_m(K_1 a)H_m'(K_o a)]}$$

$$T = \frac{k_o^2}{k_1^2} \frac{c_o^2}{c_1^2} \frac{\rho_o k_1}{\rho_1 K_o}$$

$$k_o = \omega/c_o$$

$$k_1 = \left(\frac{\omega}{c_1} - Mk_z\right)$$

$$K_o = [k_o^2 - k_z^2]^{1/2}$$

$$K_1 = [k_1^2 - k_z^2]^{1/2}$$

2. Solution of the Model

An approximate solution of the integral in equation 5 is obtained using the Method of Stationary Phase (8). By this method, the solution of the integral I_z, of the form:

$$I_z = \int_{-\infty}^{+\infty} g(\alpha) e^{iz(h(\alpha))} d\alpha \quad \text{as } z \to \infty \qquad 6)$$

is:

$$I_z = \left[\frac{2\pi}{z \left| h''(\alpha_o) \right|} \right]^{\frac{1}{2}} g(\alpha_o)\, e^{i(z(h(\alpha_o)) \pm \pi/4)} \qquad 7)$$

where:

1) α_o solves $h'(\alpha) = 0$

2) the sign in the exponential term goes as the sign of $h''(t_o)$

In order to solve equation 5 in the manner prescribed by equation 6, the following transformations are made.

Let:

$$\alpha = \sqrt{1 - \left(\frac{k_z}{k_o}\right)^2}$$

then:

1) $$dk_z = -\frac{k_o \alpha \, d\alpha}{\sqrt{1-\alpha^2}}$$

2) $$k_1 = \frac{\omega}{c_1} - Mk_z = k_o \left(\frac{c_o}{c_1} - M\sqrt{1-\alpha^2} \right)$$

3) $$K_o = [k_o^2 - k_z^2]^{\frac{1}{2}} = k_o \alpha$$

4) $$K_1 = [k_1^2 - k_z^2]^{\frac{1}{2}} = k_o \left[\left(\frac{c_o}{c_1} - M\sqrt{1-\alpha^2} \right)^2 - 1 + \alpha^2 \right]^{\frac{1}{2}}$$

the integral in equation 5 :

$$I = \int_{-\infty}^{+\infty} e^{ik_z z} H_m(k_o r)\ F_m(k_{o_1} k_1)\quad dk_z$$

becomes:

$$I = -k_o \int_{-\infty}^{+\infty} \frac{\alpha e^{ik_o z \sqrt{1-\alpha^2}}}{\sqrt{1-\alpha^2}} H_m(k_o r\alpha)\ F_m(\alpha)\ d\alpha \qquad 8)$$

In the acoustic far field, r>>1. Assuming that $k_z << k_o$, the argument of the Hankel function becomes large:

$$k_o r\alpha >> 1$$

and the Hankel function is approximated by:

$$H_m(k_o r\alpha) \approx \sqrt{\frac{2}{\pi\, k_o r\alpha}}\ e^{i(k_o r\alpha - \frac{\pi}{2}(m + \frac{1}{2}))} \qquad 9)$$

from figure 1, it is seen that:

$$r = R\cos\beta \text{ and } z = R\sin\beta$$

where:

R = distance from origin of the coordinate system to the receiver

β = angle between vector R and the projection of the vector R on the x - y plane.

The integral is then:

$$I = -\sqrt{\frac{2k_o}{\pi R\cos\beta}}\left(e^{-i\frac{\pi}{2}(m + \frac{1}{2})}\right) \int_{-\infty}^{+\infty} e^{ik_o R(\sqrt{1-\alpha^2}\sin\beta + \alpha\cos\beta)} \sqrt{\frac{\alpha}{1-\alpha^2}} F_m(\alpha)\, d\alpha \qquad 10)$$

comparing equation 10 to equation 6 :

$$z = k_o R$$

$$h(\alpha) = \sqrt{1-\alpha^2}\sin\beta + \alpha\cos\beta$$

$$g(\alpha) = \sqrt{\frac{\alpha}{1-\alpha^2}}\, F_m(\alpha)$$

α_o is evaluated from:

$$h'(\alpha_o) = \cos\beta - \frac{\alpha_o}{\sqrt{1-\alpha_o^2}}\sin\beta = 0$$

thus:

$$\alpha_o = \cos\beta \qquad 11)$$

then: $h(\alpha_o) = 1$

and: $$h''(\alpha_o) = -\frac{1}{\sin^2\beta}$$

and: $$g(\alpha_o) = \sqrt{\frac{\cos\beta}{\sin^2\beta}}\, F_m(\cos\beta)$$

The integral, as $k_o R \gg 1$, becomes:

$$I = \frac{2i}{R} e^{-im\pi/2} e^{ik_o R} F_m(\cos\beta) \qquad 12)$$

From which the expression for the far field acoustic velocity potential is evaluated:

$$\phi = \frac{Q_o e^{-i\omega t}}{4\pi R} \sum_{m=o}^{\infty} \varepsilon_m \cos m(\theta-\theta_o) e^{\frac{-im\pi}{2}} e^{ik_o R} F_m(\cos\beta) \qquad 13)$$

Where:

$$F_m(\cos\beta) = J_m(k_o r_o \cos\beta) -$$

$$\Big\{ H_m(k_o r_o \cos\beta) \Big[\rho_1 c_1^2 T_1^2 \cos\beta\, J_m(k_o a\, T_2)\, J_m'(k_o a \cos\beta)$$

$$- \rho_o c_o^2 T_2\, J_m(k_o a \cos\beta)\, J_m'(k_o a\, T_2) \Big] /$$

$$\Big[\rho_1 c_1^2 T_1^2 \cos\beta\, J_m(k_o a\, T_2)\, H_m'(k_o a \cos\beta) - \rho_o c_o^2 T_2\, H_m(k_o a \cos\beta)\, J_m'(k_o a\, T_2) \Big] \Big\} \quad 14)$$

where:

$$T_1 = \frac{c_o}{c_1} - M \sin\beta$$

$$T_2 = \Big[\Big(\frac{c_o}{c_1} - M \sin\beta \Big)^2 - \sin^2\beta \Big]^{\frac{1}{2}}$$

The total acoustic velocity potential in the far field consists of two parts:

1. The velocity potential of the incident wave:

$$\phi_{in} = \frac{Q_o e^{-i\omega t}}{4\pi R} \sum_{m=o}^{\infty} \epsilon_m \cos m(\theta-\theta_o) e^{\frac{-im\pi}{2}} e^{ik_o R} J_m(k_o r_o \cos\beta) \quad 15)$$

2. The velocity potential of the scattered wave:

$$\phi_{sc} = \frac{Q_o e^{-i\omega t}}{4\pi R} \sum_{m=o}^{\infty} \epsilon_m \cos m(\theta\ \theta_o) e^{\frac{im\pi}{2}} e^{ik_o R} X$$

$$\Big\{ \text{terms in equation 14) within brackets} \Big\} \quad 16)$$

As a check; when $r_o = o$ (source is located at the origin), the velocity potential of the incident wave reduces to:

$$\phi_{in} = \frac{Q_o e^{ik_o(R-ct)}}{4\pi R}$$

since;

$$J_m(o) = \begin{cases} 1 & m = o \\ o & m \neq o \end{cases}$$

This is the expression for the velocity potential in the far field for radiation from a point source of strength, Q_o, located at the origin of the co-ordinate system.

IV RESULTS

The total sound pressure is evaluated from the acoustic velocity potential by:

$$P_T = -\rho_o \frac{\partial}{\partial t} \phi_T$$

The incident sound pressure is evaluated from equation 15:

$$P_{in} = -\rho_o \frac{\partial \phi_{in}}{\partial t} = + \frac{i\omega \bar{Q}_o}{4\pi R} \rho_o \sum_{m=o}^{\infty} \epsilon_m \cos m(\Theta-\Theta) e^{\frac{-im\pi}{2}} e^{ik_o R} J_m(k_o r_o \cos \beta) \qquad 17)$$

The normalized sound pressure is formed from the magnitude of the ratio of the total sound pressure to the incident sound pressure. This normalized sound pressure is a measure of the influence of the shielding jet on the noise source directionality. A value of normalized sound pressure less than one indicates noise reduction; and a value of normalized sound pressure greater than one indicates amplification.

The normalized sound pressure is evaluated in the shielded zone of the jet. Thus, $\Theta-\Theta_o = \pi$ and $o < \beta < \pi/2$. For the purposes of comparison to other data, the coordinates are shifted to a set centered in the source, and illustrated in figure 2. In the nomenclature adopted in the figure, $\psi_n = o°$ is on the z-axis of the noise source, and $\psi_n = 90°$ is on the side of the jet directly opposite the source.

1. Identification of Shielding Mechanisms

The mechanisms which control the noise in the shadow of the shielding jet in the downstream region are transmission through the jet and diffraction around the jet.

In order to differentiate among the mechanisms of shielding, the normalized sound pressure is evaluated at low frequencies under the following operating conditions.

a) V_j = Jet velocity = 1552 feet/sec

b) T_j = Jet tmeperature = 1238°R

c) T_o = Ambient temperature = 530°R

d) S/D = Spacing parameter = ratio of distance from source to center of jet and jet diameter. = 2.667

The contours of normalized pressure for $10° < \psi_n < 90°$ are plotted against non-dimensional frequency parameter in figure 3. The non-dimensional frequency $k_o a$ is varied from 0.1 to 1.0

For angles, ψ_n, within the range:

$$90° > \psi_n > 70°$$

transmission of noise through the jet is dominant. The normalized sound pressure is close to 1.0 for a relatively large range of frequencies, indicating that the noise transmits easily through the jet. The normalized sound pressure curves shift toward lower frequency as the angle is decreased, which indicates that as the angle of incidence becomes more oblique, more of the incident sound is entrained within the jet and and convected downstream.

The cut-off angle:

$$\psi_{nct} = \cos^{-1} \left(\frac{c_o/c_j}{1+M}\right)$$

where:

c_o = sound speed at the ambient temperature, T_o

c_j = sound speed at jet temperature, T_j

M = jet mach numbers = V_j / c_j

is the angle beyond which, thoeretically, no sound is transmitted through the jet (4).

In the model development of the previous section, ψ_{nct} is the angle at which the parameter T_2 goes to zero in equation 14.

$$T_2 = \left[\left(\frac{c_o}{c_j} - M\cos\psi_n \right)^2 - \cos^2\psi_n \right]^{\frac{1}{2}} = 0 \text{ at } \psi_n = \psi_{nct}$$

where:

$$\psi_n = \frac{\pi}{2} - \beta$$

for the operating parameters in figure 3, the cut-off angle is:

$$\psi_{nct} = 69.9°$$

In theory, all the incident sound in the range $\psi_n > \psi_{nct}$ is transmitted through the jet, while no transmission occurs for sound incident at $\psi_n < \psi_{nct}$.

Refering to figure 3, the normalized sound pressure decreases more rapidly in the range of angles $40° < \psi_n < 70°$ than it does on the range $70° < \psi_n < 90°$. This indicates that transmission of noise through the jet is relatively efficient at $\psi_n > 70°$. While sound is transmitted through the jet at $\psi_n < 70°$, the contribution of transmitted sound decreases rapidly.

The normalized sound pressure contours reach a minimum at $\psi_n \approx 40°$. For angles less than 40°, the curves shift toward higher frequency. In this range of angles, diffraction around the jet becomes dominant. The increase in normalized sound pressure with decrease in angle is consistent with barrier theory, where decreasing the angle of incidence has the same effect as increasing the distance between the source and the barrier.

The angle at which diffraction begins to dominate is evaluated from:

$$\psi_{ncd} = \cos^{-1}\left(\frac{c_o / c_j}{M} \right)$$

This angle is the value at which the parameter T_1 in equation 14 goes to zero.

$$T_1 = \frac{c_o}{c_j} - M \cos \psi_n = 0 \quad \text{at } \psi_n = \psi_{ncd}$$

where:

$$\psi_n = \frac{\pi}{2} - \beta$$

for the operating parameters shown:

$$\psi_{ncd} = 43.4°$$

Since the transmitted noise decreases constantly for $\psi_n < \psi_{nct}$, and diffracted noise adds to the sound pressure at angles $\psi_n < \psi_{ncd}$; the angle at which the normalized sound pressure is minimum is equal to ψ_{ncd}.

Curves of normalized sound pressure for the receiver in the transmission dominated, diffraction dominated and transition zones are shown in figure 4. The frequency scale is expanded to show the differences at higher frequency.

For the receiver in the transmission dominated zone, the normalized sound pressure reduces rapidly, with frequency, to a minimum value. At higher frequencies, the sound pressure oscillates about a terminal value which is greater than the minimum.

When the receiver is in the transition zone:

$$\psi_{nct} > \psi_n > \psi_{ncd}$$

the normalized sound pressure becomes smoother. The initial decrease in sound pressure is not as rapid. The first minimum occurs at lower frequency and is not as sharp. The sound pressure is oscillatory at higher frequencies, but the period of oscillation increases.

For the receiver in the diffraction dominated zone, the normalized sound

pressure reduction becomes more broad band. No oscillation at high frequency is observed.

These general comments serve to identify the zones in which the mechanisms of transmission and diffraction control. The effects of jet operating parameters on the sound pressure in the transmission and diffraction dominated zones are discussed below.

2. Effect of Jet Operation Parameters

A. Transmission Dominant Zone

Figure 5 shows the normalized sound pressure distribution plotted against non-dimensional frequency parameter, $k_o a$, for a receiver in the transmission dominant zone:

$$90° > \psi_n > \psi_{nct}$$

a) Effect of the Mach Number

The curves on figure 5 represent a range of Mach Numbers, from 0.76 to 1.12. Generally, increasing the Mach Number shifts the curve toward lower frequency. As the Mach Number increases, the transmission zone cut-off angle, ψ_{nct}, is increased. Thus, a receiver at a fixed location is effectively moved closer to the cut-off angle; and, in so doing, sees less of the transmitted noise. The curves in figure 5 are found to collapse to one curve when plotted against:

$$k_o a \, (\psi_n - \psi_{nct})^{-.17}$$

where:

ψ_n = observer angle (radians)

$$\psi_{nct} = \cos^{-1} \left(\frac{c_o / c_j}{1+M} \right)$$

Figure 6 shows the resulting curve for the spacing ratio S/D = 2.667 from figure 5; as well as for spacing ratios, S/D = 1.000 and 5.000.

b) Effect of Spacing Ratio

As is shown in figure 6, the effect of increasing the spacing ratio is to shift the curves toward higher frequencies. These curves are found to collapse to a single curve when plotted against the normalized frequency parameter

$$(k_o a)\ (\psi_n - \psi_{nct})^{-.17}\ (\frac{S}{D})^{-.17}$$

The resulting curve is shown in figure 7. This curve is similar to one obtained in a previous report (9) for the formulation of the two dimensional model. The onset of shielding occurs at the value of the normalized parameter approximately 0.175 as was found previously. The minimum sound pressure occurs at a value of the parameter equal to 3.0, and was 2.72 in the previous analysis. The normalizing exponent, -.17, compares to the exponent, -.20, evaluated in the previous report.

B. Diffraction Dominant Zone

Figure 8 shows the normalized sound pressure as a function of frequency for a receiver in the diffraction dominant zone,

$$\psi_n < \psi_{ncd}$$

a) Effect of Mach Number.

Figure 8 shows that the effect of increasing the Mach Number is to shift the curve toward higher frequencies. The curves approach a high frequency assymptotic curve which is independent of Mach Number. The curves in figure 8 are found to collapse to one curve when plotted against:

$$k_o a\ (\psi_{ncd} - \psi_n)^{-1.96}$$

where:

ψ_n = observer angle (radians)

ψ_{ncd} = diffraction zone cut-off angle

$$= \cos^{-1}\left(\frac{c_o/c_j}{M}\right) \quad \text{(radians)}$$

This relationship is valid only for $M > \frac{c_o}{c_j}$.

For $M < \frac{c_o}{c_j}$, ψ_{ncd} does not exist; and there is no diffraction dominant zone.

The curves in figure 8, for spacing ratio S/D = 2.667 are plotted against the normalizing parameter in figure 9. Also shown are similar curves for S/D = 1.000, and 5.000 .

b) Effect of Spacing Ratio.

From figure 9, the effect of increasing the spacing ratio is to shift the curves toward higher frequencies. As the distance between the source and the shielding jet increases, the minimum normalized pressure ratio which is approached at high frequency also increases.

The minimum sound pressure ratio is found to be related to the spacing ratio by:

$$\left|\frac{P_T}{P_{in}}\right|_{min} \approx .59 \log_{10} (S/D) + .15$$

c) Temperature

ψ_{ncd} is related to jet temperature in that the speed of sound in the jet is a function of $(T_j)^{\frac{1}{2}}$. Thus, as the jet temperature is decreased, the cut-off angle is also decreased. The expected result of decreasing the jet temperature is to

shift the curve toward lower frequency. This result is shown in figure 10. The plots in figure 10 also show that the curves coalesce to a high frequency assymptote which is temperature independent. The assymptote is, however, dependent on spacing ratio.

Figure 11 shows the two curves normalized against the parameter:

$$k_o a \, (\psi_{ncd} - \psi_n)^{1.96}$$

where:

$$\psi_{ncd} = f \, (T_j^{-\frac{1}{2}})$$

The dashed line on the figure is the best fit curve from figure 9 for the corresponding spacing ratio.

3. Comparison to Experimental Results,

The analytical model is compared to experimental results by Kantola (10) and plotted in figure 12. The condition evaluated is :

a. T_j = 1238° R

b. V_j = 1519 feet/sec

c. S/D = 2.667

d. ψ_n = 30°, 60°

The analytical model shows some agreement in form with the experimental data. The onset of shielding occurs at lower frequency for ψ_n = 30° than it does for ψ_n = 60°. As the jet axis is approached, the agreement between the analytical and experimental improves, with the significant difference being at high frequencies. The analytical model shows that normalized sound pressure increases for $k_o a > 10$. This indicates an upper frequency limit on shielding. The experimental results indicate no such upper limit in the range of frequencies investigated.

The major discrepancy between the analytical and experimental results occur at greater angles of incidence. This is felt to be due to the point source approximation of the source jet. The jet noise source is more realistically considered to be a distribution of point sources along the jet axis. The downstream sources are contributing to the sound pressure measured in the shielded zone. From the previous discussion on transmission through the shielding jet, the sound incident on the jet at $\psi_n < 70°$ is transmitted more readily than sound incident at $\psi_n < 70°$. In general then, sound is transmitted upstream more efficiently than downstream because the angle of incidence is greater. Thus, the receiver at $\psi_n = 60°$ "sees" more of the downstream noise sources than does the receiver located closer to the jet axis. The point source approximation for the source jet breaks down as the angle of incidence increases.

V CONCLUSIONS

In the shadow of the shielding jet in the downstream region, the mechanisms which control the noise are transmission and diffraction.

Between the angles $90 > \psi_n > \psi_{nct}$ transmission through the jet dominates. In this zone, the normalized sound pressure is close to 1. over a relatively large range of frequencies. As frequency is increased, the sound pressure decreases rapidly to a minimum value: at still higher frequencies, the sound pressure is oscillatory, indicating phase interference due to passage through the jet. The effect of increasing Mach or decreasing the spacing ratio number is to shift the curves toward lower frequency. The normalized sound pressure is represented by one curve when plotted against the normalized parameter

$$(k_o a)\left[(\psi_n - \psi_{nct}) \times \frac{S}{D}\right]^{-.17}$$

The resulting curve compares favorably with a similar curve obtained from the two dimensional formulation. The value of the exponent, -.17, indicates that the sound pressure is relatively insensitive to changes in the jet operating parameters.

Between the angles $\psi_{nct} > \psi_n > \psi_{ncd}$, the influence of transmission decreases and the influence of diffraction increases. The normalized sound pressure curves shift toward lower frequency. The oscillatory nature of the sound pressure at high frequency is reduced.

At angles, $\psi_n < \psi_{ncd}$, diffraction is the dominant mechanism. Since transmission constantly decreases for angles, $\psi_n < \psi_{nct}$ and diffraction around the jet increases for $\psi_n < \psi_{ncd}$, the minimum sound pressure occurs at $\psi_n = \psi_{ncd}$. The diffraction zone cut-off angle

$$\psi_{ncd} = \cos^{-1}\left(\frac{c_o/c_j}{M}\right)$$

is strongly dependent on the ratio of sound speed, $\frac{c_o}{c_j}$, and the Mach Number, M.

For values,

$$\frac{c_o/c_j}{M} > 1$$

ψ_{ncd} does not exist, and the shielded region does not contain a diffraction dominant zone.

In the diffraction dominated zone, the attenuation of the source noise is relatively broad band. At low frequency, the normalized sound pressure curves are shifted toward higher frequencies as the jet axis is approached. This result is consistent with barrier theory. At high frequencies, the normalized sound pressure approaches an assymptotic value, and none of the oscillatory character is observed. This indicates that at high frequencies, the sound incident on the shielding jet is scattered away from the shadow zone.

In the diffraction dominant zone, low frequency reduction of the sound pressure is degraded as Mach Number is increased. At high frequency, the normalized sound pressure tends toward an assymptotic value which is independent of Mach Number. Increasing Mach Number increases the cut-off angle, ψ_{ncd} . The shape of the normalized sound pressure curve is found to be related to the included angle between the observer location and the cut-off, ψ_{ncd} . When the sound pressure is plotted against the normalized frequency parameter:

$$k_o a \, (\psi_{ncd} - \psi_n)^{-1.96}$$

the curves become Mach Number independent.

Increasing jet temperature also increases the cut-off angle, since:

$$\frac{c_o}{c_j} = \left[\frac{T_o}{T_j}\right]^{\frac{1}{2}}$$

Thus, when the normalized sound pressure is plotted against the parameter

$$k_o a \, (\psi_{ncd} - \psi_n)^{-1.96}$$

the curves become independent of temperature.

The value of the exponent, -1.96, indicates that the sound pressure in the diffraction dominant zone is more sensitive to changes in jet operating parameters, than is the sound pressure in the transmission dominant zone.

The curves which result from normalization in terms of the cut-off angle are strongly dependent on the spacing ratio, S/D. The curves are shifted toward higher frequency as the spacing increases. This result is expected from barrier theory. The curves also appear to approach high frequency assymptotic values which increase as the spacing increases. The minimum sound pressure is found to be related to the spacing ratio by:

$$\left| \frac{P_T}{P_{in}} \right|_{min} \approx .59 \log_{10} \left(\frac{S}{D}\right) + .15$$

for the range of spacing ratios

$$1.000 < \frac{S}{D} < 5.000$$

The analytical model compares to experimental results favorably for angles of incidence close to the jet axis. The discrepencies that occur at greater angles of incidence are felt to arise from the difference between the single point source approximation in the model and the distributed source configuration of the real jet.

REFERENCES

1. Ribner, H.S., "Reflection, Transmission, and Amplification of Sound by a Moving Medium", JASA vol. 29, no. 4, p. 435

2. Miles, J.W., "On the Reflection of Sound at an Interface of Relative Motion", JASA vol. 29, no. 2, p. 226

3. Yeh, C., "Reflection and Transmission of Sound Waves by a Moving Fluid Layer", JASA vol. 41, no. 4, p. 817

4. Yeh, C., "A Further Note on the Reflection and Transmission of Sound Waves by a Moving Fluid Layer", JASA vol. 43, no. 6, p. 1454

5. Parthasarathy, S.P., Cuffel, R.F.,and Massier, P.F., "Twin Jet Study, Final Report", Jet Propulsion Laboratory: California Institute of Technology, Pasadena, California, November 3, 1978

6. Candel, S. and Julienne, A., "Shielding and Scattering by a Jet Flow", 3rd AIAA Aero-Acoustics Conference, Palo Alto, California. July, 20-23, 1976

7. Gerhold, C.H., "Development of an Analytical Model of Twin Jet Shielding". Progress report for NASA Grant NAG-1-11. June 19, 1980.

8. Jefferies, H. and Jefferies, B., Methods of Mathematical Physics, Cambridge University Press, 1956

9. Gerhold, C.H., "Analytical Study of Twin Jet Shielding - Two Dimensional Model". Progress report for NASA NAG Grant 1-11. August 14, 1980

10. Kantola, R.A., "Shielding Aspects of Heated Twin Jet Noise", AIAA 4th Aero-Acoustics Conference Atlanta, Georgia, October 3-5, 1977.

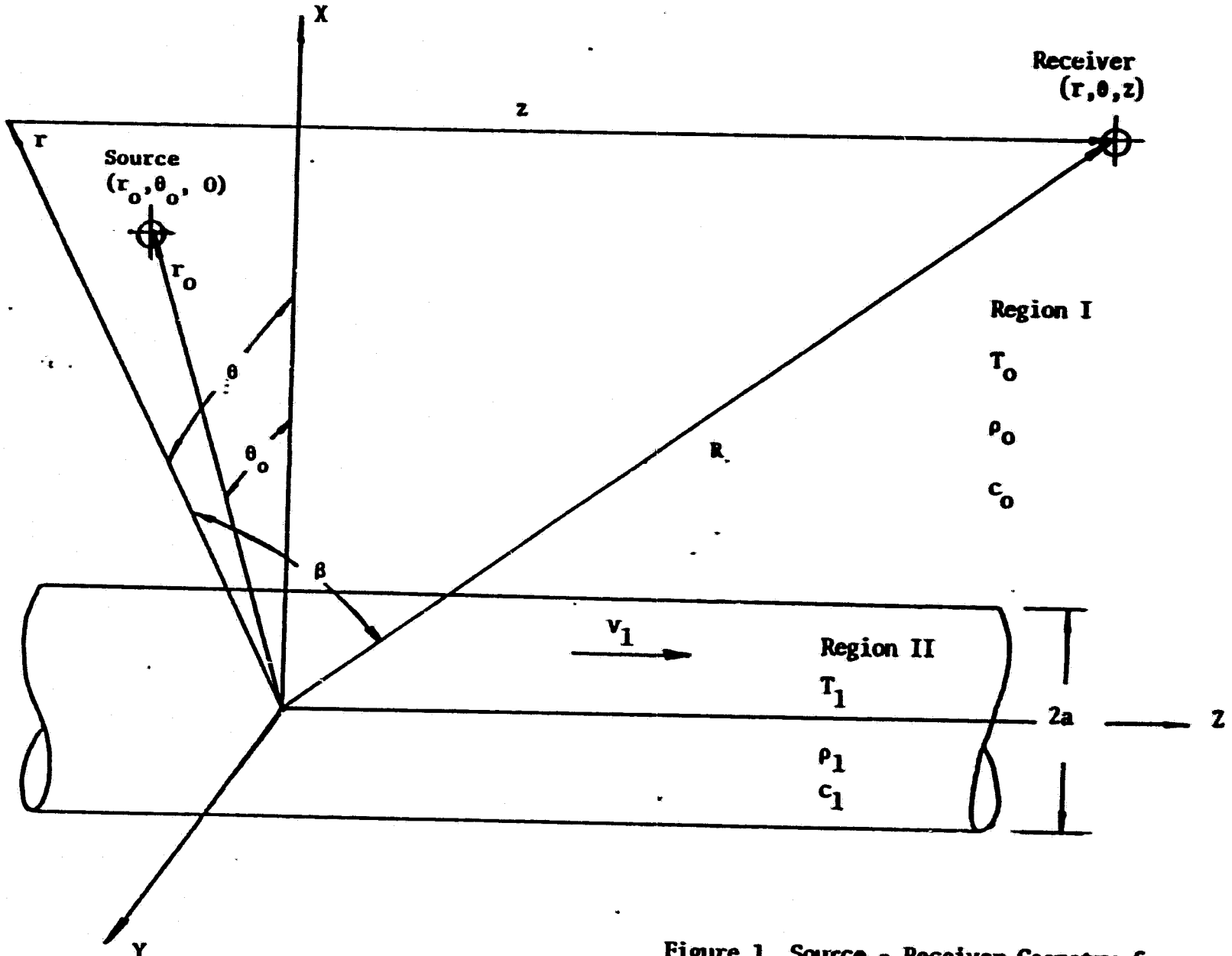

Figure 1 Source - Receiver Geometry for Jet Shielding Analysis.

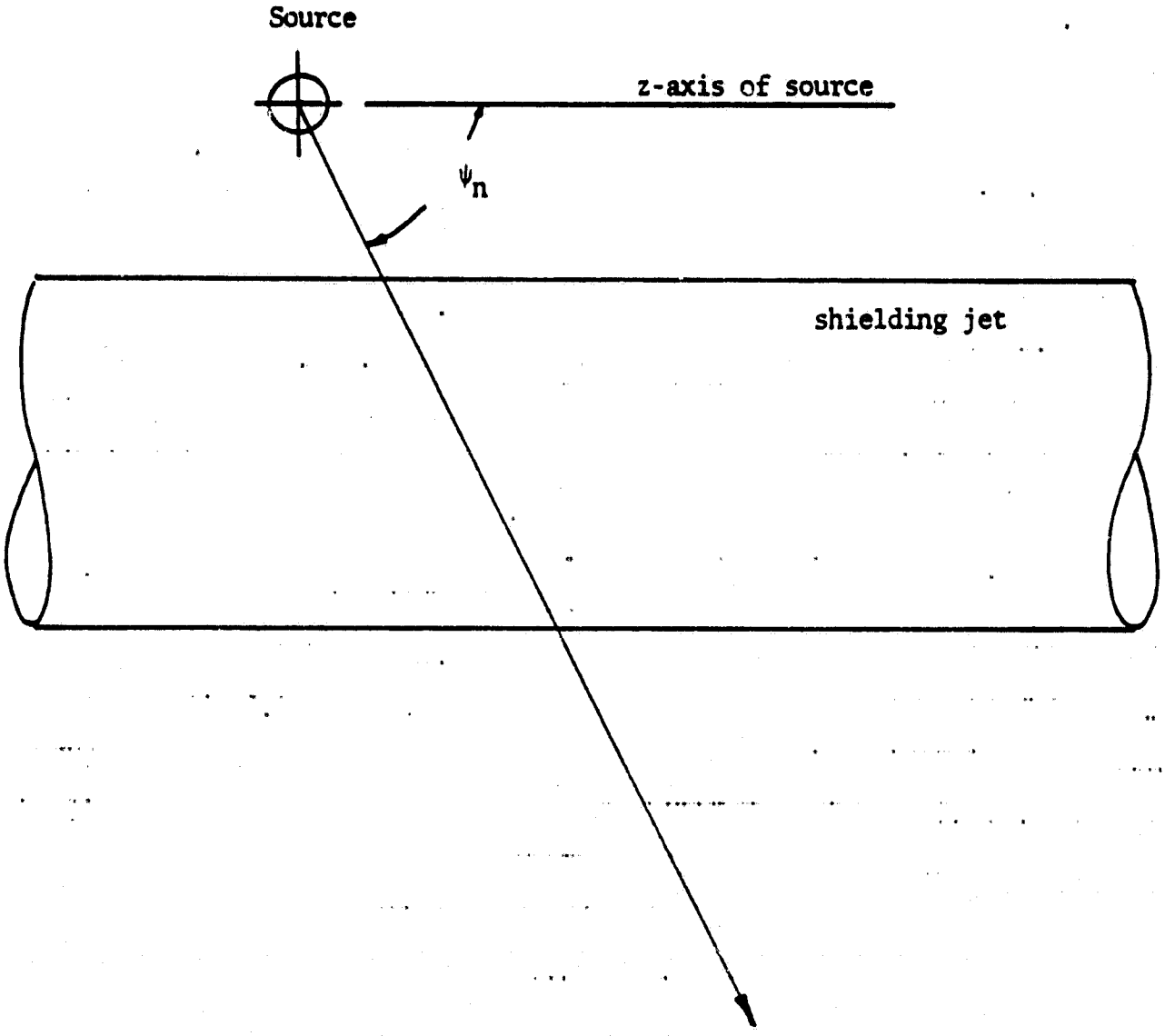

Figure 2 Definition of Angle in Coordinates centered on Noise source

Figure 3. Distribution of Normalized Sound Pressure in Shielded Zone.

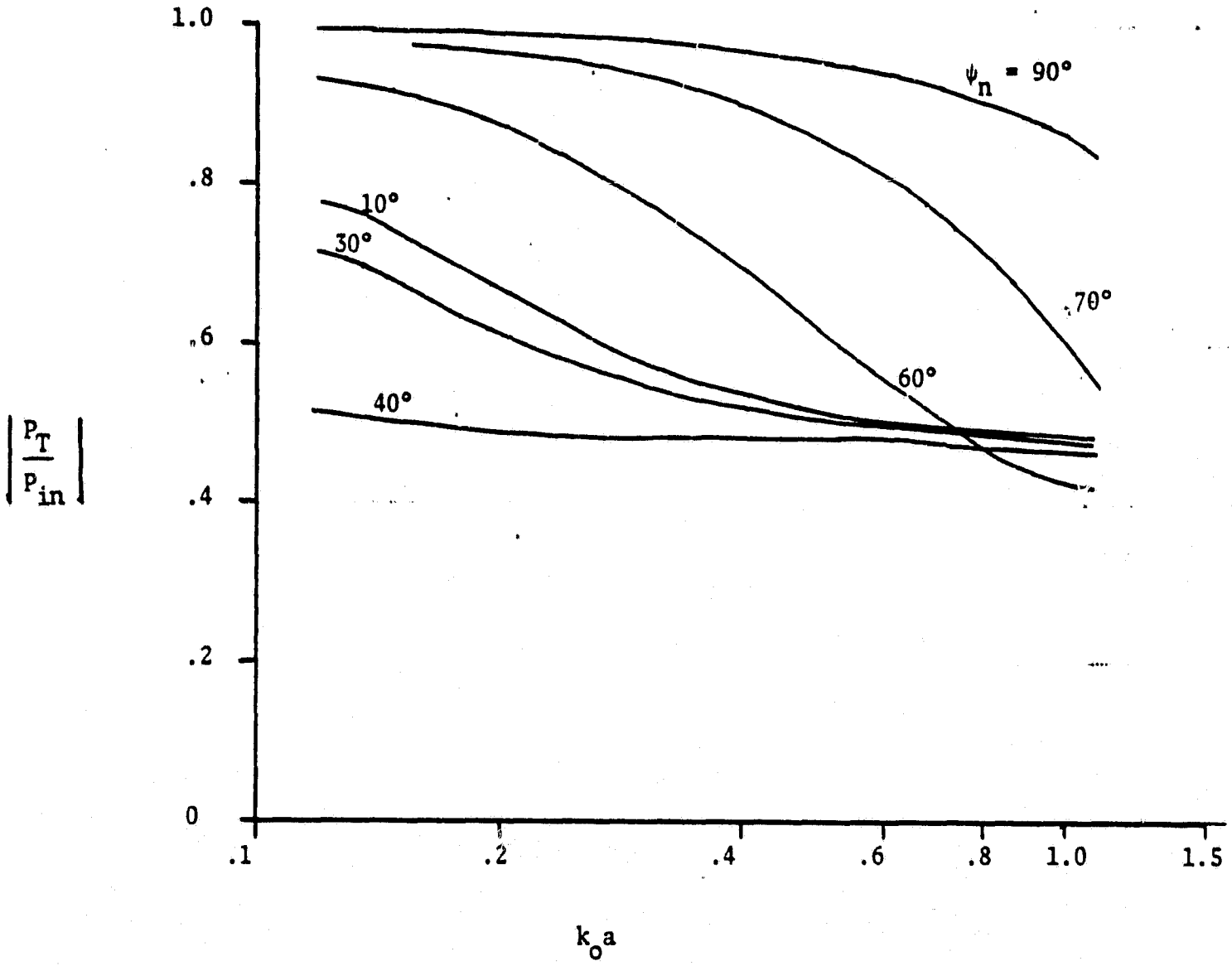

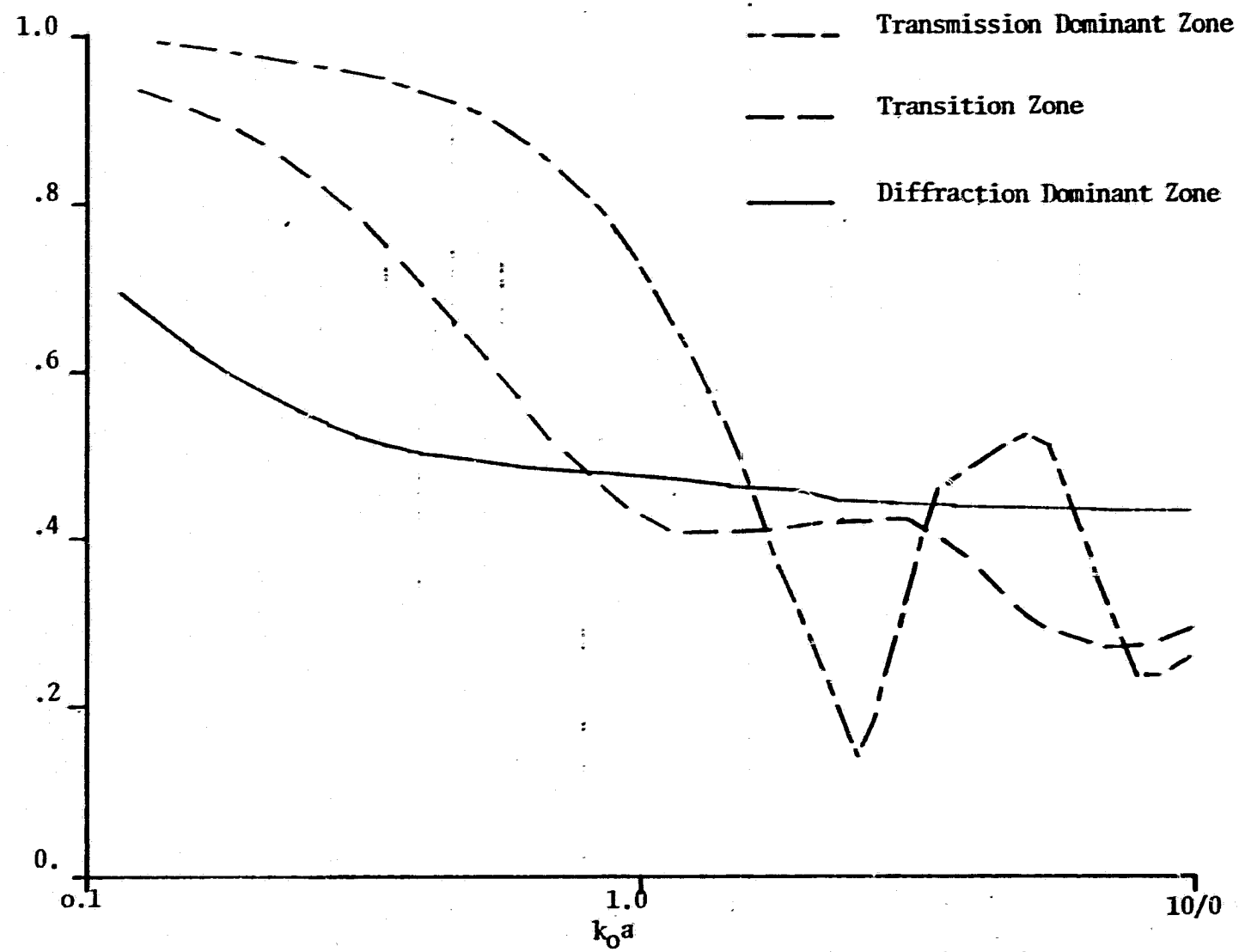

Figure 4. Variation of Normalized Sound Pressure with Non-dimensional Frequency. Receiver in Shadow Region of Shielding Jet.

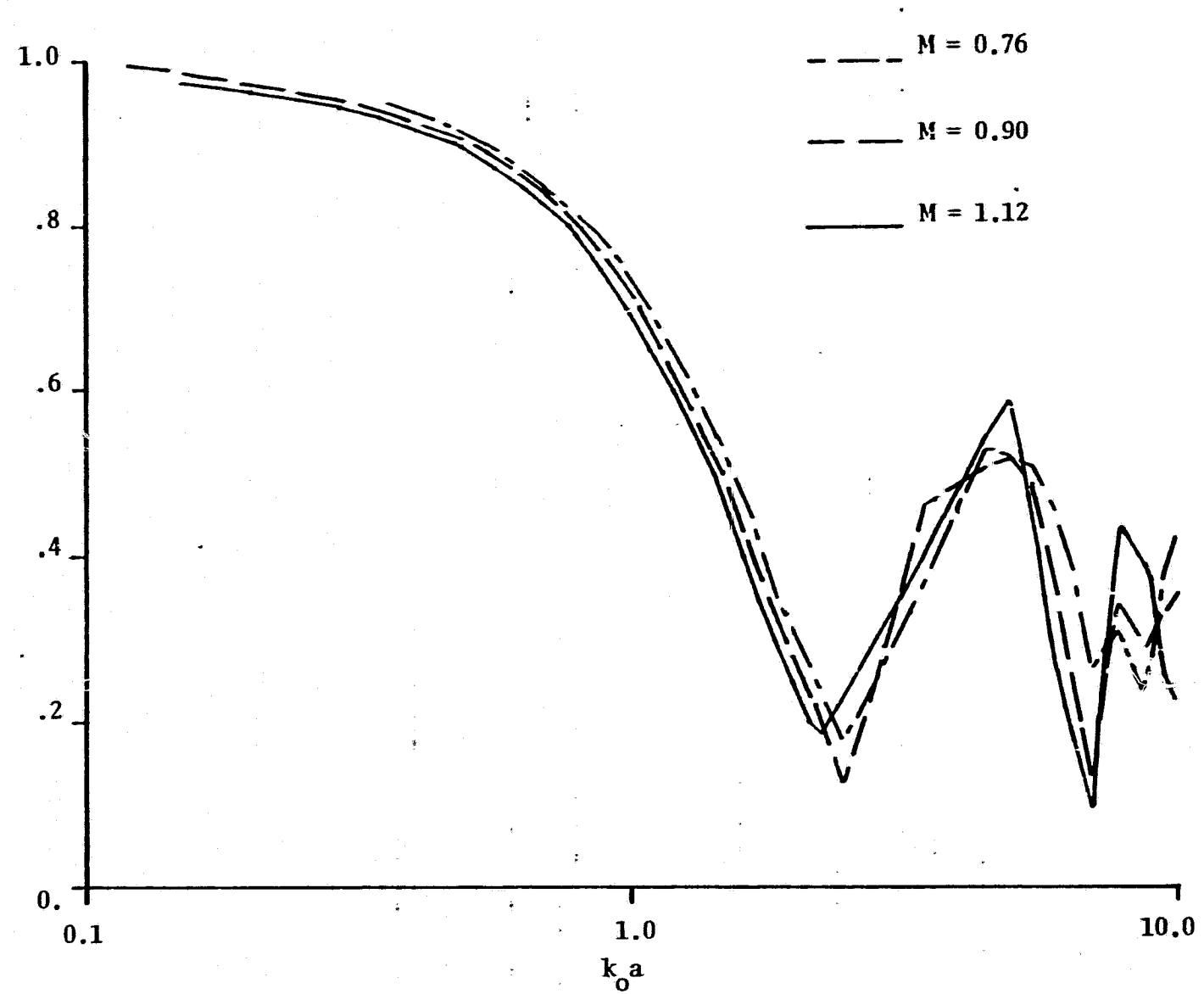

Figure 5. Variation of Normalized Sound Pressure with Non-dimensional Frequency Receiver in Transmission Dominant Zone. Spacing Ratio, S/D = 2.667

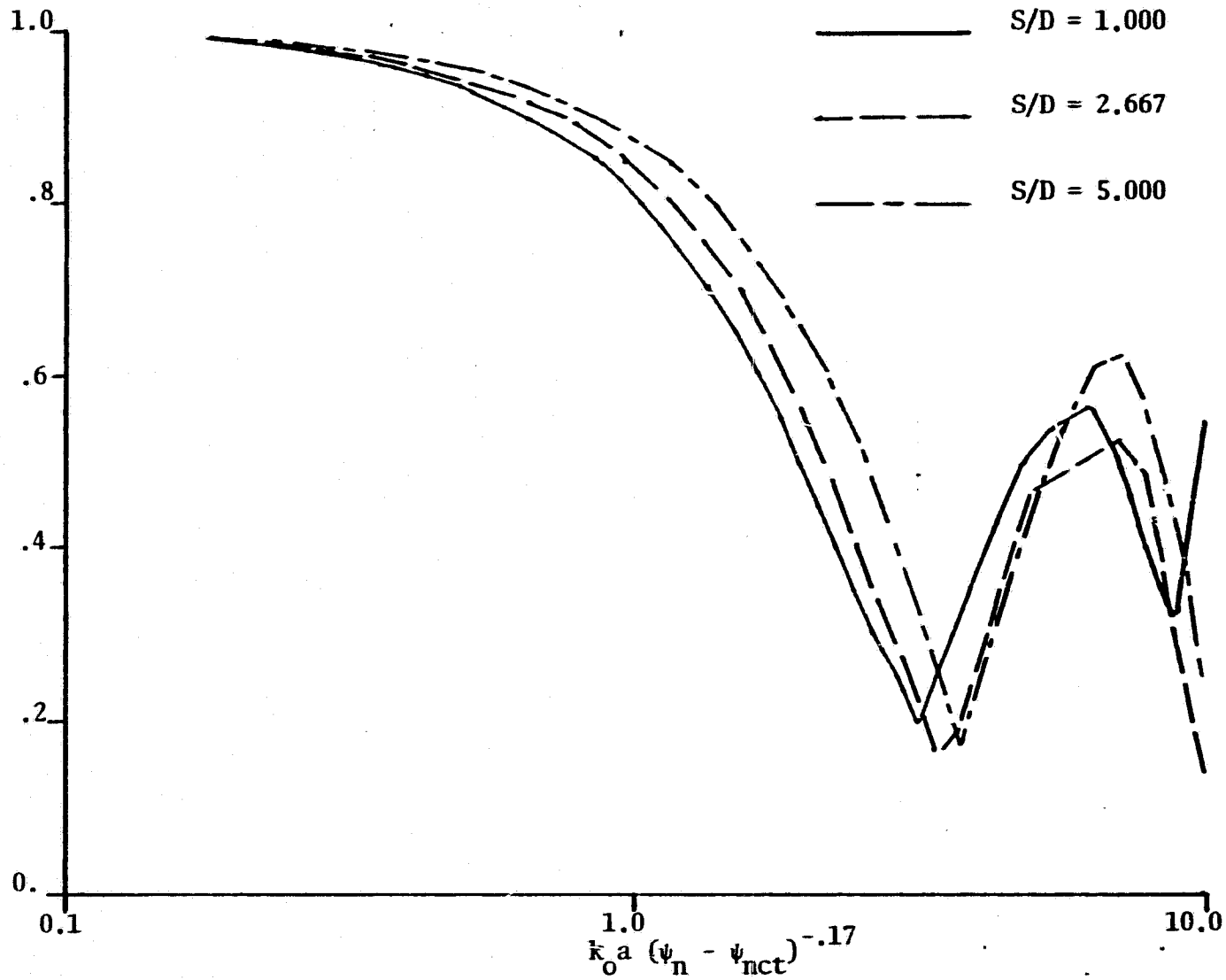

Figure 6. Variations of Normalized Sound Pressure with Normalized Frequency Parameter. Receiver in Transmission Dominant Zone.

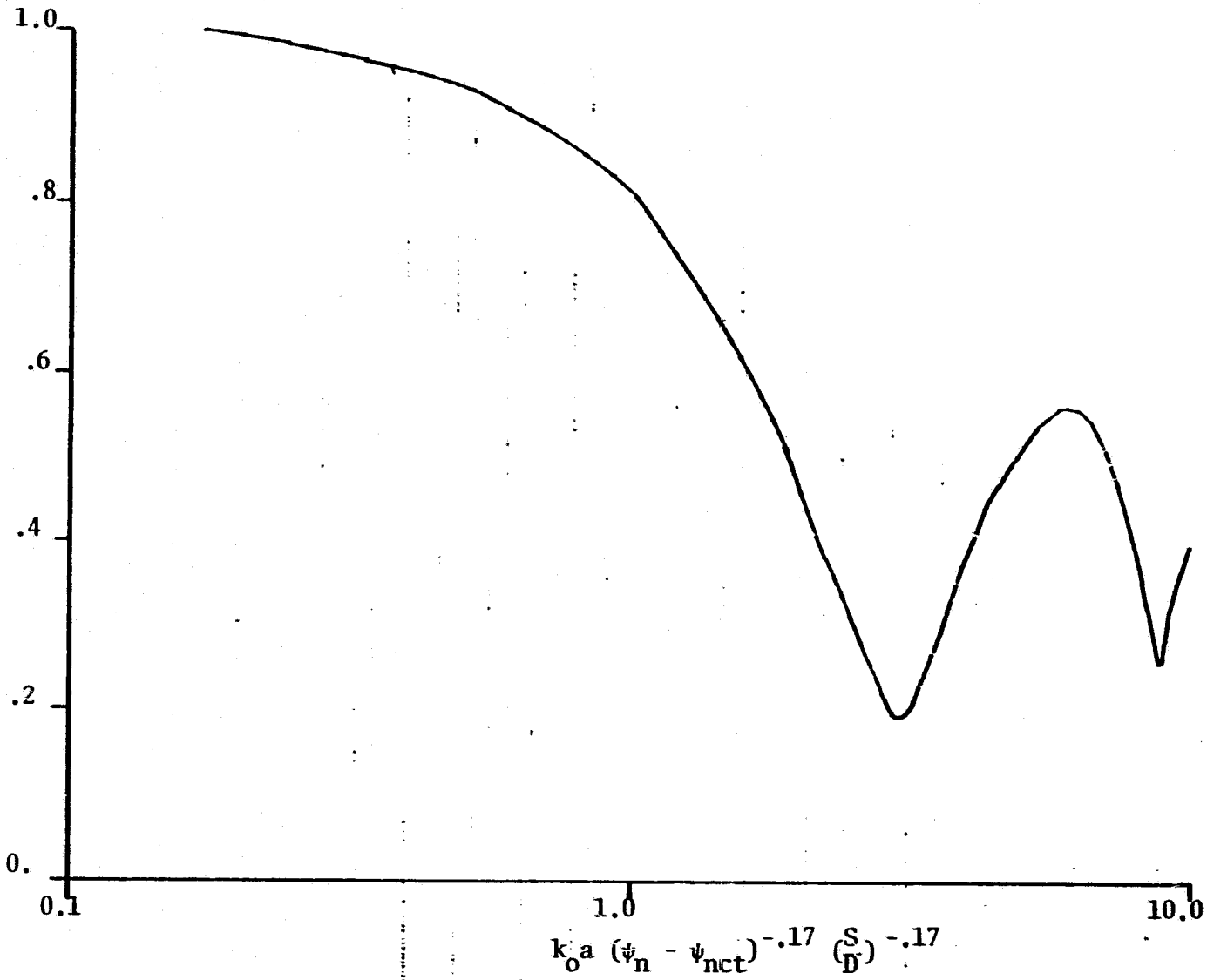

Figure 7. Variation of Normalized Sound Pressure with Normalized Frequency Parameter, all Spacing Ratios. Receiver in Transmission Dominant Zone.

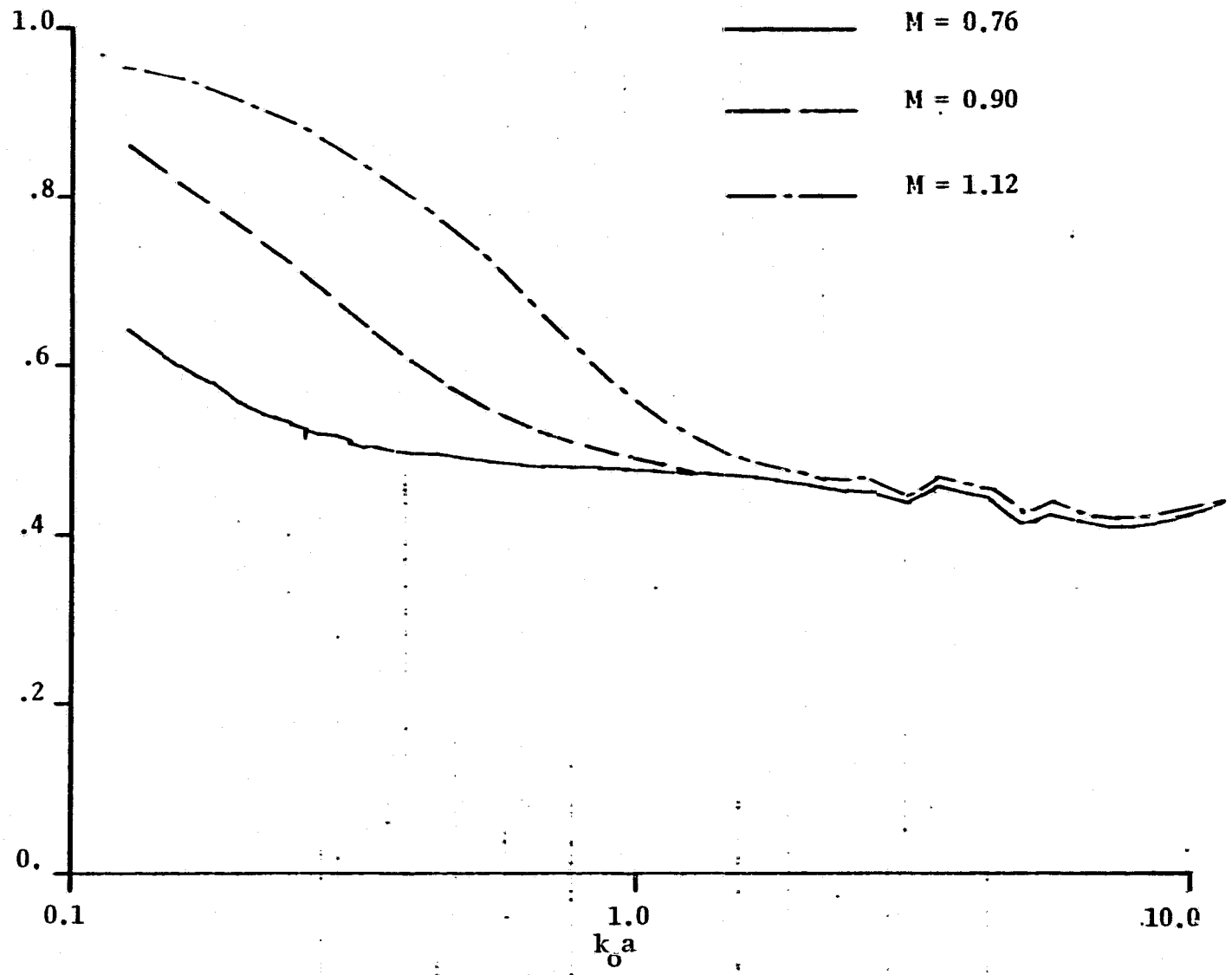

Figure 8. Variation of Normalized Sound Pressure with Non-dimensional Frequency. Receiver in Diffraction Dominant Zone. Spacing Ratio, $\frac{S}{D} = 2.667$

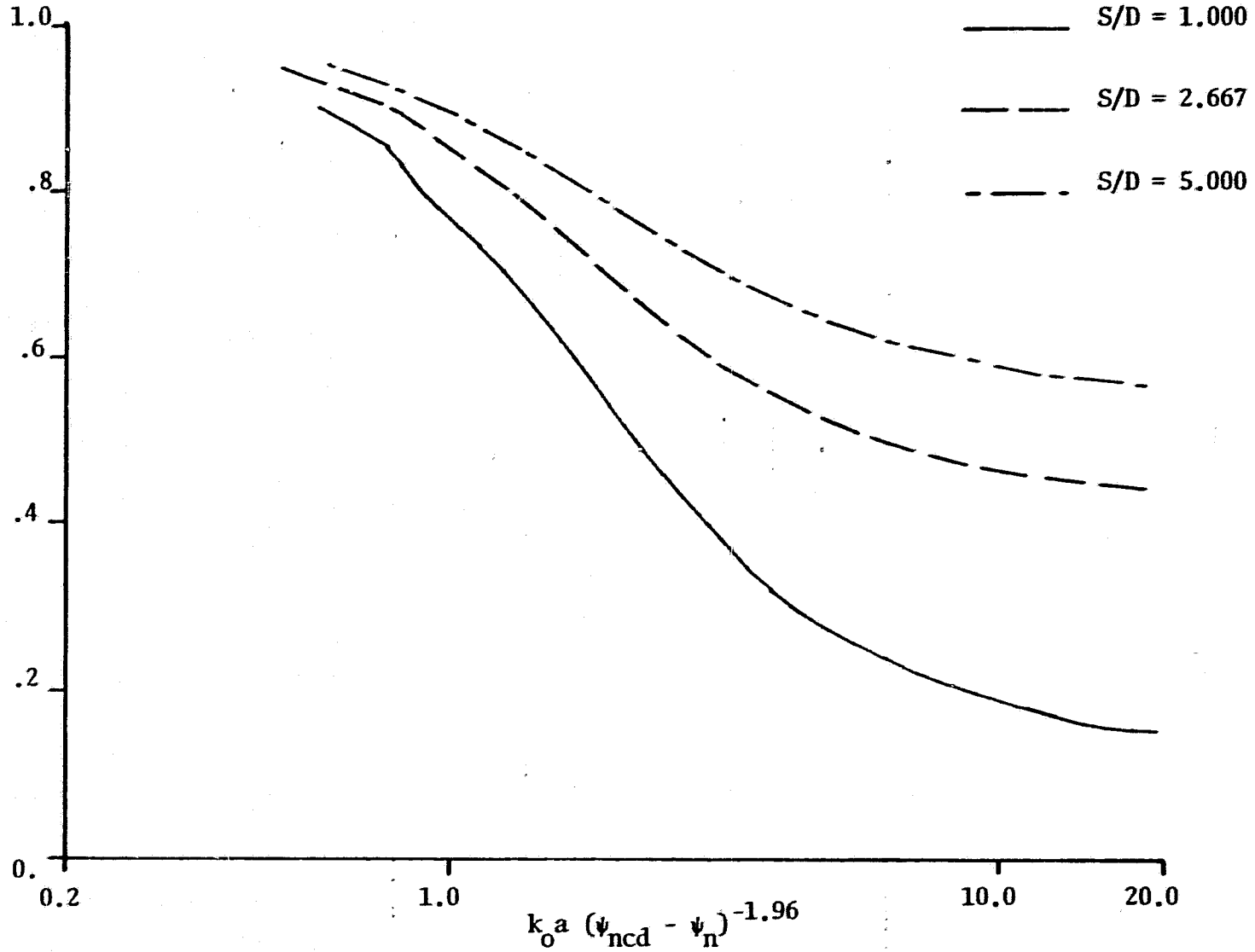

Figure 9. Variation of Normalized Sound Pressure with Normalized Frequency Parameter. Receiver in Diffraction Dominant Zone.

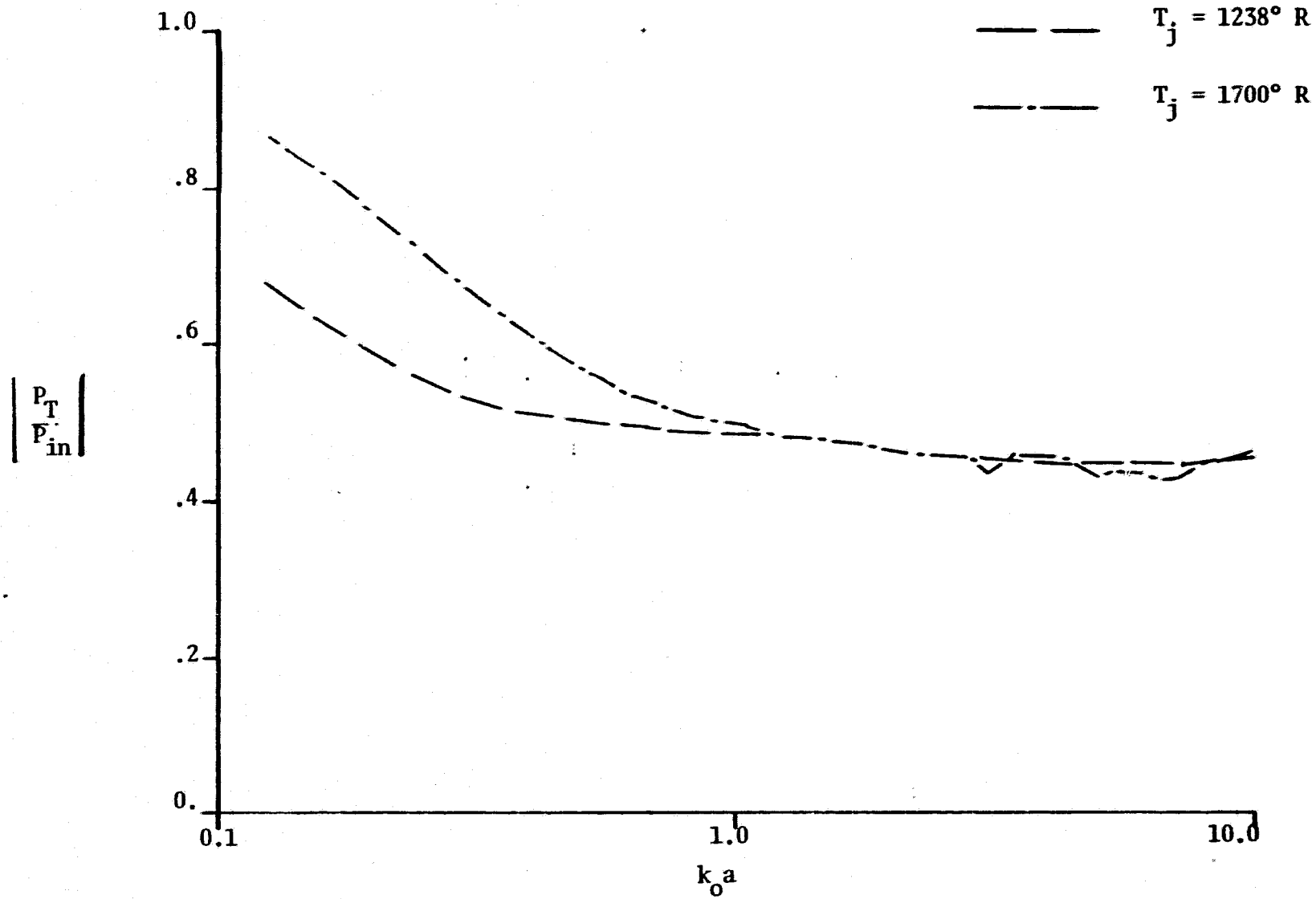

Figure 10. Variation of Normalized Sound Pressure with Non-dimensional Frequency . Receiver in Diffraction Dominant Zone. Spacing Ratio, $\frac{S}{D}$ = 2.667.

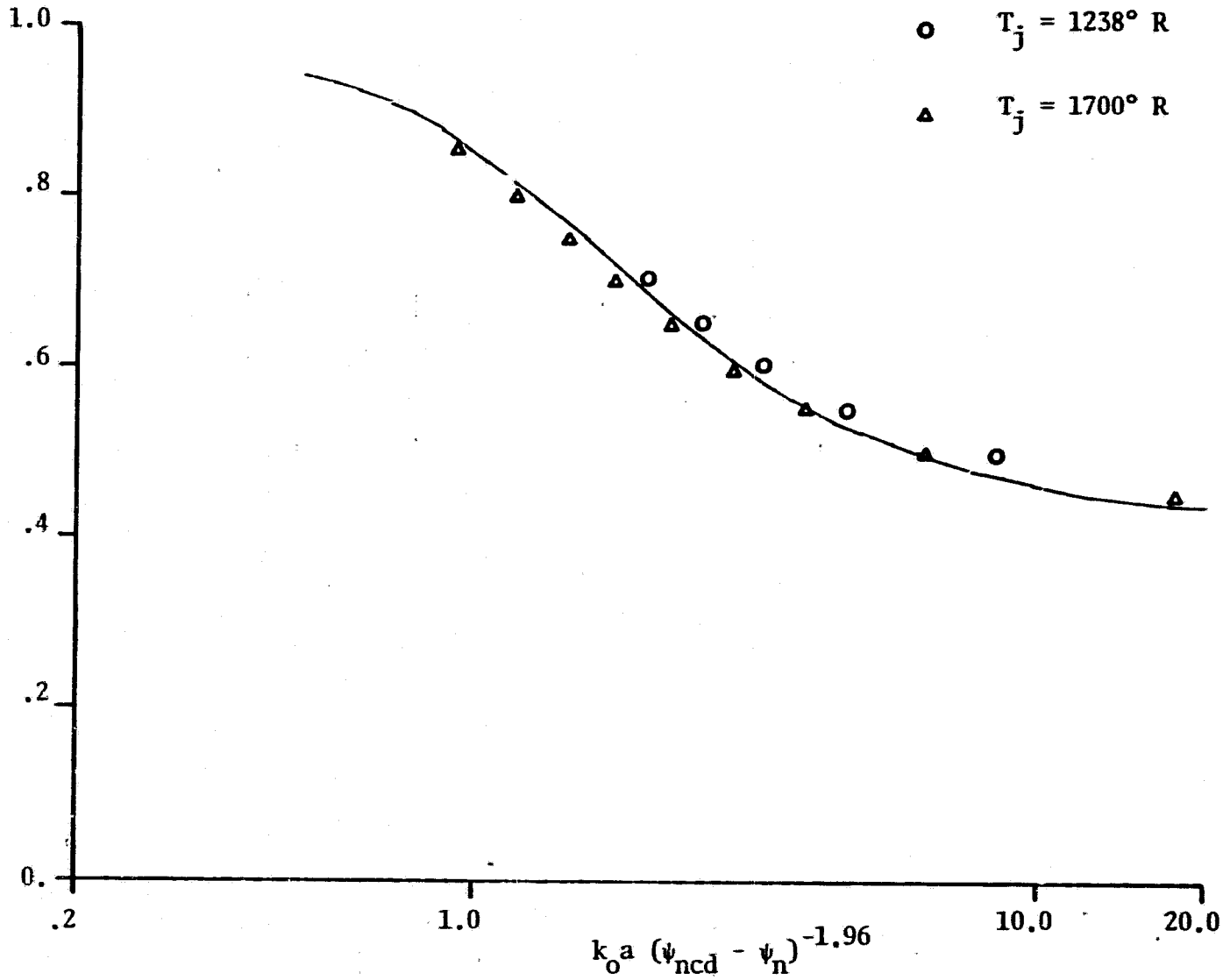

Figure 11. Plot Showing Normalization of Jet Temperature Effect. Solid Line is Normalized Sound Pressure Contour for S/D = 2.667, from Figure 9.

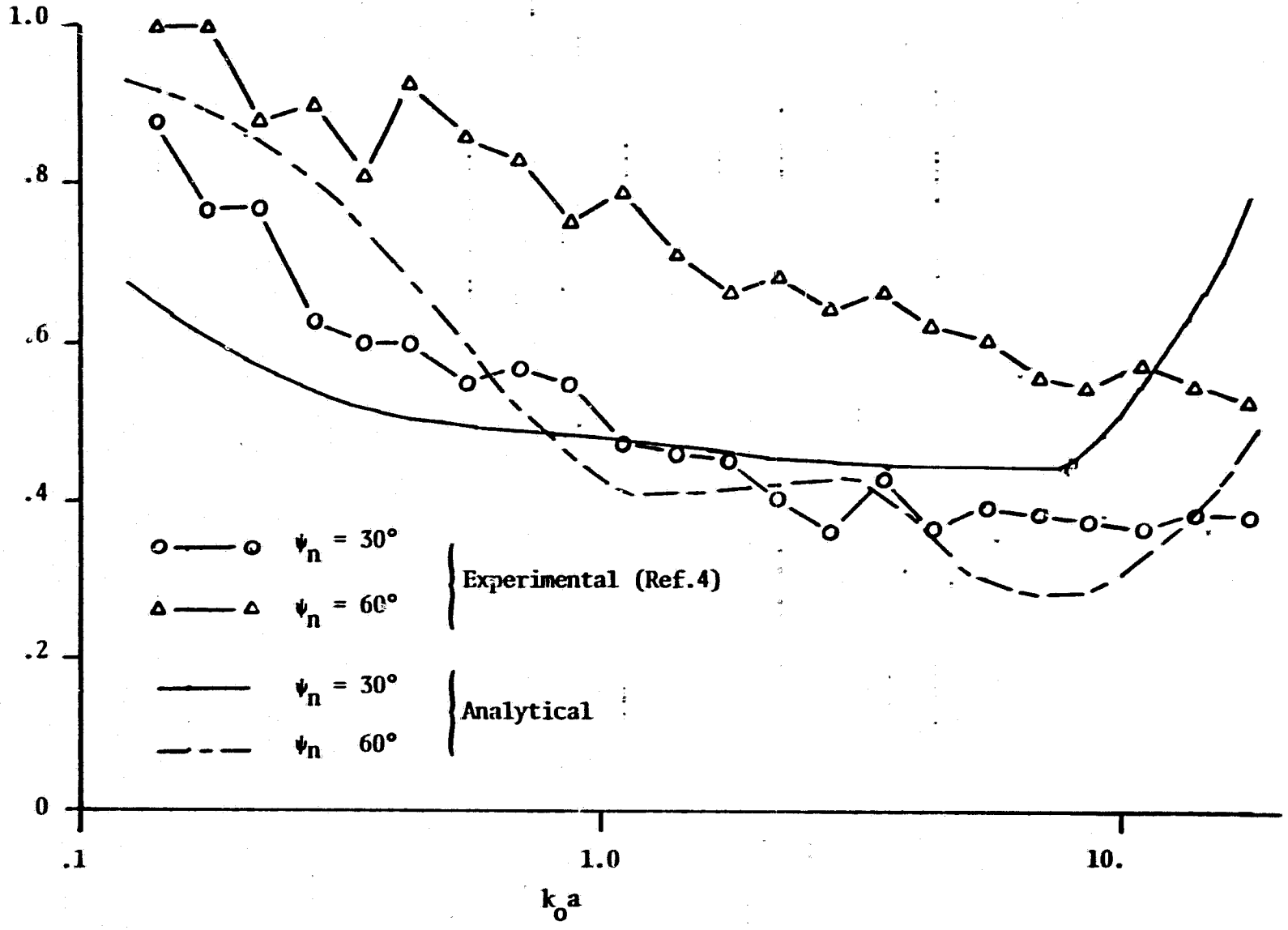

Figure 12. Comparison of Analytical to Experimental Jet Shielding